

The evolution of chaos in active galaxy models with an oblate or a prolate dark halo component

Nicolaos D. Caranicolas and Euaggelos E. Zotos^{*}

Department of Physics, Section of Astrophysics, Astronomy and Mechanics, Aristotle University of Thessaloniki, GR-541 24, Thessaloniki, Greece

Received 2009 Jun 10, accepted 2009 Nov 6

Published online 2010 Mar 12

Key words chaos - galaxies: kinematics and dynamics - methods: numerical

The evolution of chaotic motion in a galactic dynamical model with a disk, a dense nucleus and a flat biaxial dark halo component is investigated. Two cases are studied: (i) the case where the halo component is oblate and (ii) the case where a prolate halo is present. In both cases, numerical calculations show that the extent of the chaotic regions decreases exponentially as the scale-length of the dark halo increases. On the other hand, a linear relationship exists between the extent of the chaotic regions and the flatness parameter of the halo component. A linear relationship between the critical value of the angular momentum and the flatness parameter is also found. Some theoretical arguments to support the numerical outcomes are presented. An estimation of the degree of chaos is made by computing the Lyapunov Characteristic Exponents. Comparison with earlier work is also made.

© 2010 WILEY-VCH Verlag GmbH & Co. KGaA, Weinheim

1 Introduction

Observational data show that disk galaxies are often surrounded by massive and extended dark matter haloes. The best tool to study dark matter haloes in galaxies are the rotation curves derived from neutral hydrogen (see e.g. Meurer et al. 1996; Dinshaw et al. 1998; Shull et al. 1998; Oppenheimer et al. 2001; McLin et al. 2002; Penton et al. 2002; Steidel et al. 2002; Cote et al. 2005). On the other hand, numerical simulations suggest that dark matter galactic haloes are not only spherical but also may be oblate, prolate or triaxial (Merritt & Fridman 1996; Cooray 2000; Kunihito et al. 2000; Olling & Merrifield 2000; Jing & Suto 2002; Wechsler et al. 2002; Kasun & Evrard 2005; Allgood et al. 2006; Capuzzo-Dolcetta et al. 2007; Wang et al. 2009; Evans et al. 2009; Caranicolas & Zotos 2009). The variety of the shapes of galactic haloes strongly indicates that the structure of these objects plays an important role in the orbital behavior and, generally, in the dynamics of a galaxy.

In two earlier papers (Caranicolas 1997; Papadopoulos & Caranicolas 2006) we have studied axially symmetric or non axially symmetric active galaxy models with an additional spherical halo component. In both cases, it was observed that the presence of the spherical halo had as a result to reduce the area in the phase space occupied by the chaotic orbits. Therefore, it would be of significant interest to investigate the behavior of orbits in an active galaxy with a biaxial halo. On this basis, we have decided to study the motion in a disk galaxy model with an oblate or a prolate dark halo component. Particular interest will be given to the study of the regular or chaotic character of orbits and its

connection to the physical parameters of the system, such as the flatness, the core radius of the halo component and the conserved component of the angular momentum. Furthermore, we shall use the Lyapunov Characteristic Exponent (L.C.E) (see Lichtenberg & Lieberman 1992) in order to estimate and compare the degree of chaos in each case.

The dynamical model is presented in Sect. 2. Two cases are distinguished. The case when an oblate and the case when a prolate halo component is present. In Sect. 3 we study the behavior of orbits when an oblate or a prolate halo component is present. In the same section, numerically found relationships between the extent of the chaotic regions and the physical parameters of the system are presented. In Sect. 4 some semi-theoretical arguments are used in order to explain the numerically obtained results. We close with Sect. 5 where a discussion and the conclusions of this research are given and a comparison with previous work is made.

2 Description of the dynamical model

There are three components in our dynamical model. The disk-halo, the dense nucleus and the dark halo component. The disk-halo component is represented by the potential

$$V_d(r, z) = \frac{-M_d}{R}, \quad (1)$$

where $R^2 = b^2 + r^2 + (\alpha + \sqrt{h^2 + z^2})^2$. Here (r, z) are the usual cylindrical coordinates, M_d is the mass, b is the core radius of the disk-halo, α is the disks scale length and h corresponds to the disk's scale height. The dense nucleus

^{*} Corresponding author: e-mail: evzotos@astro.auth.gr

is represented by the spherical potential

$$V_n(r, z) = \frac{-M_n}{(r^2 + z^2 + c_n^2)^{1/2}}, \quad (2)$$

where M_n is the mass and c_n is the scale length of the nucleus. For the dark halo component we use the logarithmic potential

$$V_h(r, z) = \frac{v_0^2}{2} \ln(r^2 + \beta z^2 + c_h^2), \quad (3)$$

where β is the flatness parameter, while c_h stands for the scale length of the dark halo component. The parameter v_0 is used for the consistency of the galactic units. We have chosen this potential because Eqs. (1) and (2) represent a modified version of the analytical potential used successfully by Caranicolas & Innanen (1991) to describe the motion in an active disk galaxy. Furthermore, Eq. (3) is used because we believe that potential (3) is suitable for the description of the motion in a dark halo as it produces a flat rotation curve (see Binney & Tremaine 2008). In this research, we shall use a system of galactic units, where the unit of length is 1 kpc, the unit of time is 0.977×10^8 yr and the unit of mass is $2.325 \times 10^7 M_\odot$. The velocity unit is 10 km/s, while G is equal to unity. In the above units we use the values: $v_0 = 20$, $\alpha = 3$, $b = 6$, $h = 0.2$, $M_d = 5000$, $M_n = 400$, $c_n = 0.25$, while β and c_h are treated as parameters. The total potential responsible for the motion of a test particle (star) of unit mass in the galaxy is

$$V_t(r, z) = V_d + V_n + V_h. \quad (4)$$

As the total potential $V_t = V_t(r, z)$ is axially symmetric and the L_z component of the angular momentum is conserved we use the effective potential

$$V_{eff}(r, z) = \frac{L_z^2}{2r^2} + V_t(r, z), \quad (5)$$

in order to study the motion in the meridian (r, z) plane. The equations of motion are

$$\dot{r} = p_r, \quad \dot{z} = p_z, \quad \dot{p}_r = -\frac{\partial V_{eff}}{\partial r}, \quad \dot{p}_z = -\frac{\partial V_{eff}}{\partial z}, \quad (6)$$

where the dot indicates derivative with respect to the time. The corresponding Hamiltonian is written as

$$H = \frac{1}{2}(p_r^2 + p_z^2) + V_{eff}(r, z) = E, \quad (7)$$

where p_r and p_z are the momenta, per unit mass, conjugate to r and z , while E is the numerical value of the Hamiltonian, which is conserved. Eq. (7) is an integral of motion, which indicates that the total energy of the test particle is conserved.

Orbit calculations are based on the numerical integration of the equations of motion, which was made using a sharp Bulirsh-Stöer FORTRAN routine in double precision. By the term sharp we mean that all subroutines of the numerical integration code are in double precision. The accuracy of the calculations was checked by the constancy of the energy integral, which was conserved up to the twelfth significant figure.

3 Orbit calculations when a biaxial halo component is present

In this section we shall study the behavior of orbits when a biaxial halo is present. We shall use the classical method of the Poincaré (r, p_r) , $z = 0, p_z > 0$ phase plane in order to determine the regular or chaotic character of motion. Two cases will be studied: (a) the system has a spherical or oblate halo, that is when $1 \leq \beta < 2$ and (b) the system has a prolate halo, that is when $0.1 \leq \beta < 1$. The value of c_h is in the range $8.5 \leq c_h \leq 21$.

3.1 Model with an oblate halo

Figure 1a-b shows the (r, p_r) phase plane when (a) $\beta = 1.3$ and (b) $\beta = 1.8$. The value of c_h is 8.5, while the values of all the other parameters are $v_0 = 20$, $\alpha = 3$, $b = 6$, $h = 0.2$, $M_d = 5000$, $M_n = 400$, $c_n = 0.25$ and $L_z = 10$. Here, we must note that all the initial conditions are taken inside the limiting curve. This curve contains all the invariant curves in the (r, p_r) , $z = 0, p_z > 0$ phase plane and can be obtained from (7) by setting $z = p_z = 0$ (see Papadopoulos & Caranicolas 2006). Thus, we take the values of r and p_r inside the limiting curve, while the value of p_z is found from the energy integral (7). As one can see the majority of the phase plane is covered by chaotic orbits. Regular orbits are confined mainly near the central parts of the phase plane. There are also some smaller islands produced by secondary resonances. One observes that in both cases there is a single chaotic sea. This chaotic sea is larger in the case when $\beta = 1.8$. This suggests that the flatness parameter of the halo plays an important role on the character of motion. Our numerical calculations indicate that the chaotic region in disk galaxies with dense nuclei increases when the flatness parameter β of the halo increases, provided that all the other parameters are kept constant. We shall come to this point later in the next section.

Figure 2a-b shows the (r, p_r) phase plane when (a) $c_h = 11$ and (b) $c_h = 18.5$. The value of β is 1.7, while all the other parameters are as in Fig. 1. Again, the majority of orbits are chaotic in both cases. Here, we see that when $c_h = 11$ the chaotic sea is larger. This indicates that the scale length of the halo plays also an important role on the character of motion. We observe that the extent of the chaotic regions in the phase plane decreases as c_h increases, when all the other parameters are kept constant. Therefore, we conclude that the chaotic regions in active disk galaxies are larger when a dense halo component is present. Figure 3 shows the relationship between the percentage of the area $A\%$ covered by chaotic orbits in the phase plane and c_h when $\beta = 1.7$. We see that $A\%$ decreases exponentially as c_h increases. Here, we must notice that the whole area of the phase plane is reduced and becomes smaller as c_h increases.

Figure 4a-d shows four representative orbits. Figure 4a shows a regular orbit when $\beta = 1$ and $c_h = 8.5$. The initial

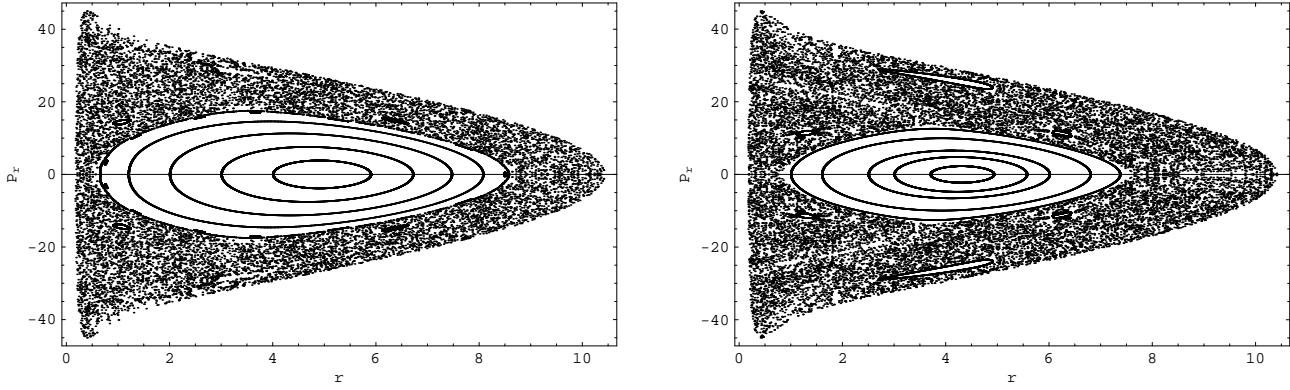


Fig. 1 (a-b): The (r, p_r) phase plane when (a, left) $\beta = 1.3$ and (b, right) $\beta = 1.8$. The value of c_h is 8.5, while the values of all the other parameters are: $v_0 = 20, \alpha = 3, b = 6, h = 0.2, M_d = 5000, M_n = 400, c_n = 0.25$ and $L_z = 10$.

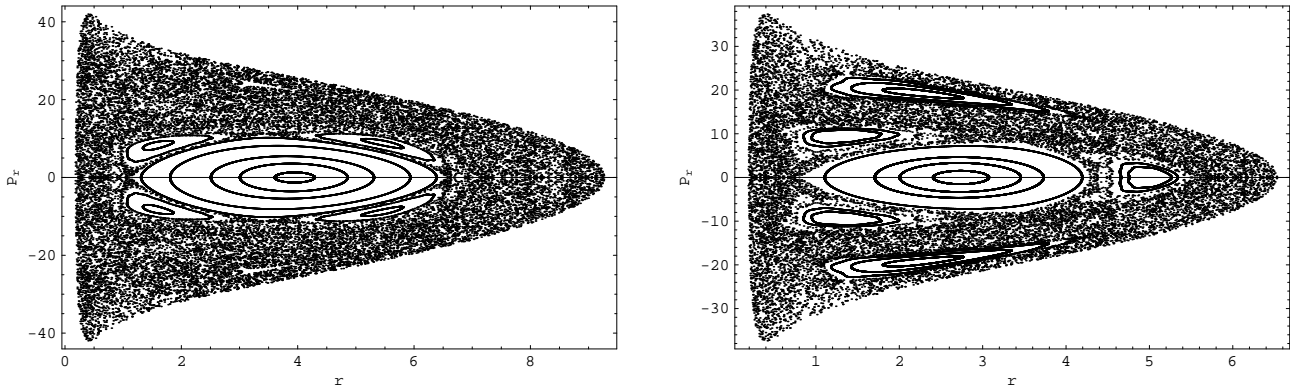


Fig. 2 (a-b): The (r, p_r) phase plane when (a, left) $c_h = 11$ and (b, right) $c_h = 18.5$. The value of β is 1.7, while the values of all the other parameters are as in Fig. 1.

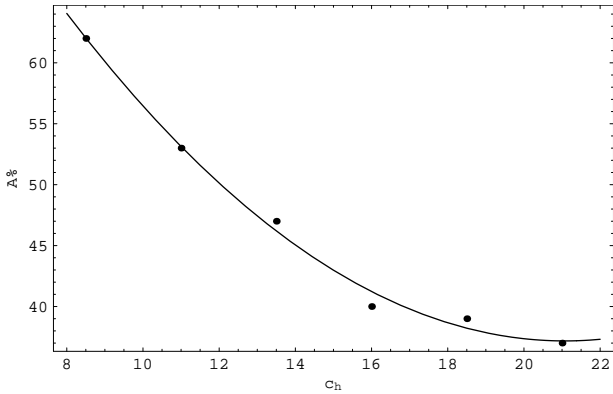


Fig. 3 A plot of the percentage of the area $A\%$ in the phase plane covered by chaotic orbits vs. c_h when $\beta = 1.7$

conditions are: $r_0 = 3, z_0 = 0, p_{r0} = 30$. The value of p_{z0} is found from the energy integral (7) for all orbits. Figure 4b shows a regular orbit when $\beta = 1.7$ and $c_h = 13$. The initial conditions are: $r_0 = 6, z_0 = 0, p_{r0} = 0$. In Fig. 4c a quasi periodic orbit is shown. Here, $\beta = 1.9$ and $c_h = 8.5$. The initial conditions are: $r_0 = 9, z_0 = 0, p_{r0} = 0$. This orbit is characteristic of the 4:3 resonance. A chaotic orbit is given in Fig. 4d. The value of β is 1.6, while $c_h = 8.5$.

The initial conditions are: $r_0 = 5, z_0 = 0, p_{r0} = 20$. All orbits were calculated for a time period of 100 time units. The value of energy is $E = 600$, while the values of all the other parameters are: $v_0 = 20, \alpha = 3, \beta = 6, h = 0.2, M_d = 5000, M_n = 400$ and $c_n = 0.25$. The value of L_z is equal to 10.

In order to have an estimation of the degree of chaos from a different point of view, we computed the L.C.E in the chaotic sea for each of the corresponding (r, p_r) phase planes for a time period of 10^5 time units for different values of β and c_h . Our numerical experiments suggest that the L.C.E is in the range from about 0.36 to about 0.43, when $c_h = 8.5$ and $1 \leq \beta < 2$, while it is in the range from about 0.40 to about 0.55, when $\beta = 1.7$ and $8.5 \leq c_h \leq 21$. Figure 5 shows the L.C.E for the chaotic orbit of Fig. 4d.

3.2 Model with a prolate halo

Figure 6a-b shows the (r, p_r) phase plane when (a) $\beta = 0.6$ and (b) $\beta = 0.2$. The value of c_h is 8.5, while the values of all the other parameters are: $v_0 = 20, \alpha = 3, \beta = 6, h = 0.2, M_d = 5000, M_n = 400, c_n = 0.25$ and $L_z = 10$. Let us start from Fig. 6a. In this case we see that the majority of the phase plane is covered by regular orbits. A consider-

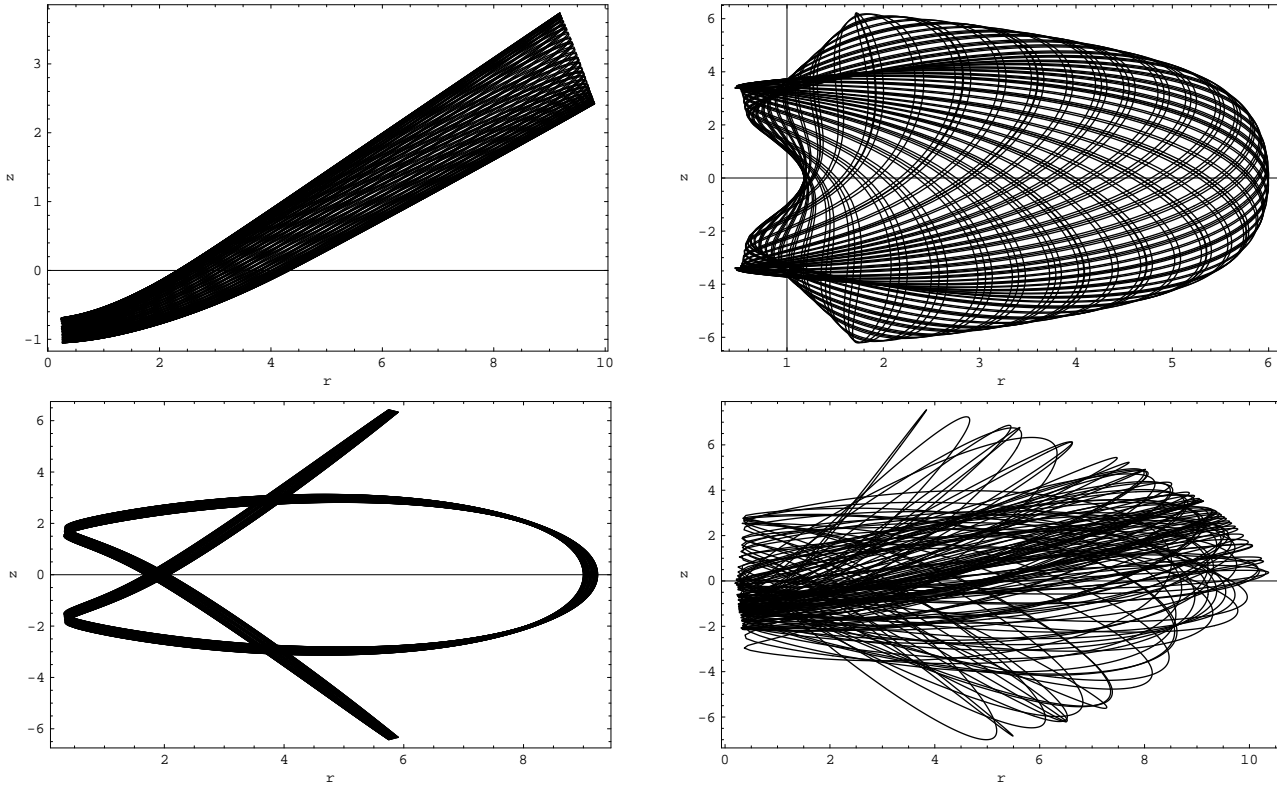


Fig. 4 (a-d): Orbits when the system has an oblate dark halo. (a, upper left): a regular orbit when $\beta = 1.0$ and $c_h = 8.5$. The initial conditions are: $r_0 = 3, z_0 = 0, p_{r0} = 30$. (b, upper right): a regular orbit when $\beta = 1.7$ and $c_h = 13$. The initial conditions are: $r_0 = 6, z_0 = 0, p_{r0} = 0$. (c, lower left): a quasi periodic orbit when $\beta = 1.9$ and $c_h = 8.5$. The initial conditions are: $r_0 = 9, z_0 = 0, p_{r0} = 0$. (d, lower right): a chaotic orbit. The value of β is 1.6, while $c_h = 8.5$. The initial conditions are: $r_0 = 5, z_0 = 0, p_{r0} = 20$. The value of p_{z0} is found from the energy integral (7) for all orbits. The values of all the other parameters are given in text.

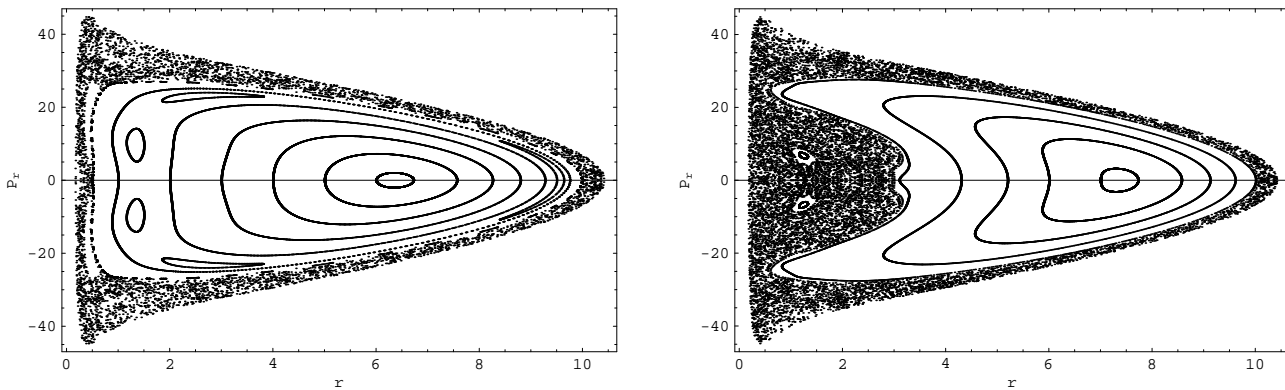


Fig. 6 (a-b): The (r, p_r) phase plane when (a, left) $\beta = 0.6$ and (b, right) $\beta = 0.2$. The value of c_h is 8.5, while the values of all the other parameters are: $v_0 = 20, \alpha = 3, \beta = 6, h = 0.2, M_d = 5000, M_n = 400, c_n = 0.25$ and $L_z = 10$.

able chaotic layer is present and it is confined in the outer parts of the phase plane. In Fig. 6b we have the case where $\beta = 0.2$. Here again the majority of the orbits are regular and secondary resonances are also present. The main difference from Fig. 6a is that now the chaotic layer has become a chaotic sea. This suggests that the flatness parameter of the prolate halo plays also an important role on the character of motion. We shall come to this point later in the next section.

Figure 7a-b shows the (r, p_r) phase plane when (a) $c_h = 11$ and (b) $c_h = 18.5$. The value of β is 0.6, while all the other parameters are as in Fig. 1. Again, the majority of orbits are regular. A careful observation shows that when $c_h = 11$ the chaotic sea is larger than when $c_h = 18.5$. Note again that the whole area of the phase plane is reduced and becomes smaller as c_h increases. Figure 8 shows the relationship between the percentage of the area $A\%$ covered by

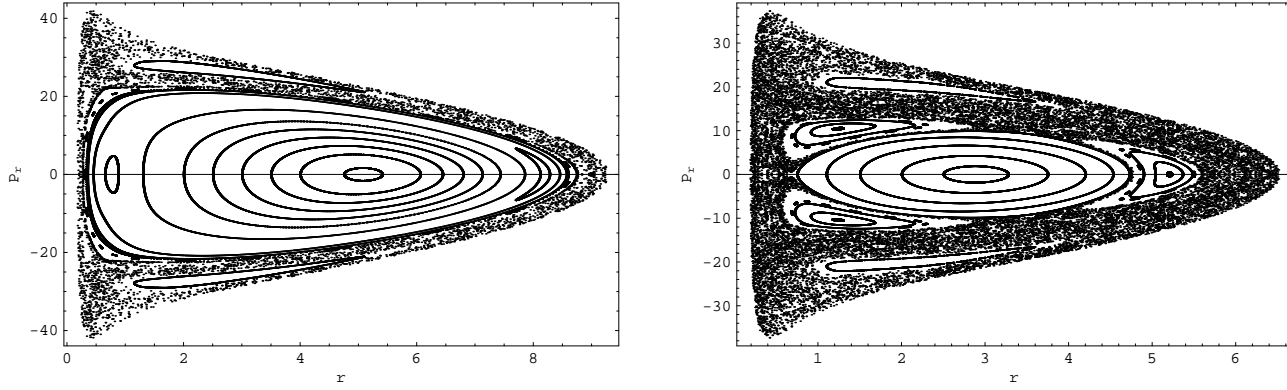


Fig. 7 (a-b): The (r, p_r) phase plane when (a, left) $c_h = 11$ and (b, right) $c_h = 18.5$. The value of β is 0.6, while the values of all the other parameters are as in Fig. 6.

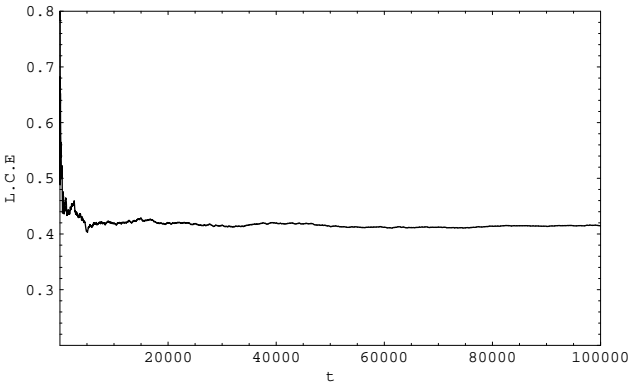


Fig. 5 Evolution of the L.C.E with the time for the chaotic orbit shown in Fig. 4d.

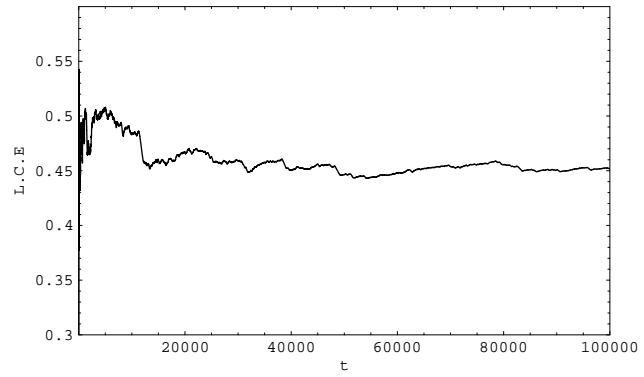


Fig. 10 Evolution of the L.C.E with the time for the chaotic orbit shown in Fig. 9d.

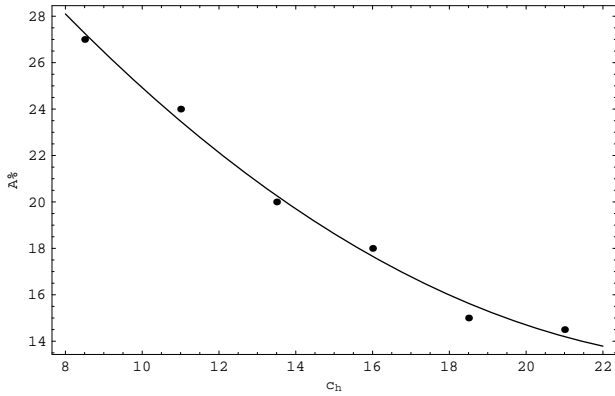


Fig. 8 A plot of the percentage of the area $A\%$ in the phase plane covered by chaotic orbits vs. c_h when $\beta = 0.7$. The values of all the other parameters are given in text.

chaotic orbits in the phase plane and c_h , when $\beta = 0.7$. We observe that $A\%$ decreases exponentially as c_h increases. This behavior is similar to that found in Fig. 3 for the oblate halo component.

In Figure 9a-d we present four representative orbits. Figure 9a shows an orbit when $\beta = 0.2$ and $c_h = 8.5$. The initial conditions are: $r_0 = 1.3, z_0 = 0, p_{r0} = 6$. This or-

bit produces the upper small island shown in Fig. 5b. Figure 6b shows a regular orbit when $\beta = 0.3$ and $c_h = 8.5$. The initial conditions are: $r_0 = 5, z_0 = 0, p_{r0} = 0$. The orbit is characteristic of the 2:1 resonance. In Fig. 9c a quasi periodic orbit is shown. Here, $\beta = 0.6$ and $c_h = 16$. The initial conditions are: $r_0 = 6.5, z_0 = 0, p_{r0} = 0$. The orbit is characteristic of the 4:3 resonance. A chaotic orbit is given in Fig. 9d. The value of β is 0.2, while $c_h = 8.5$. The initial conditions are: $r_0 = 2, z_0 = 0, p_{r0} = 0$. All orbits were calculated for a time period of 100 time units. The value of energy is $E = 600$, while the values of all the other parameters are: $v_0 = 20, \alpha = 3, \beta = 6, h = 0.2, M_d = 5000, M_n = 400, c_n = 0.25$ and $L_z = 10$.

Computation of the L.C.E in the case of the prolate halo for different values of β and c_h , shows that the L.C.E is in the range from about 0.40 to about 0.55, when $c_h = 8.5$ and $0.1 \leq \beta < 0.9$, while it is in the range from about 0.51 to about 0.57, when $\beta = 0.6$ and $8.5 \leq c_h \leq 21$. Figure 10 shows the L.C.E for the chaotic orbit of Fig. 9d.

Let us now come to see how the percentage of the chaotic regions in the phase plane is connected with the flatness parameter β . The results are given in Fig. 11 when $0.1 \leq \beta < 2$, that is, for both the prolate and the oblate halo together. There are three different linear parts in this fig-

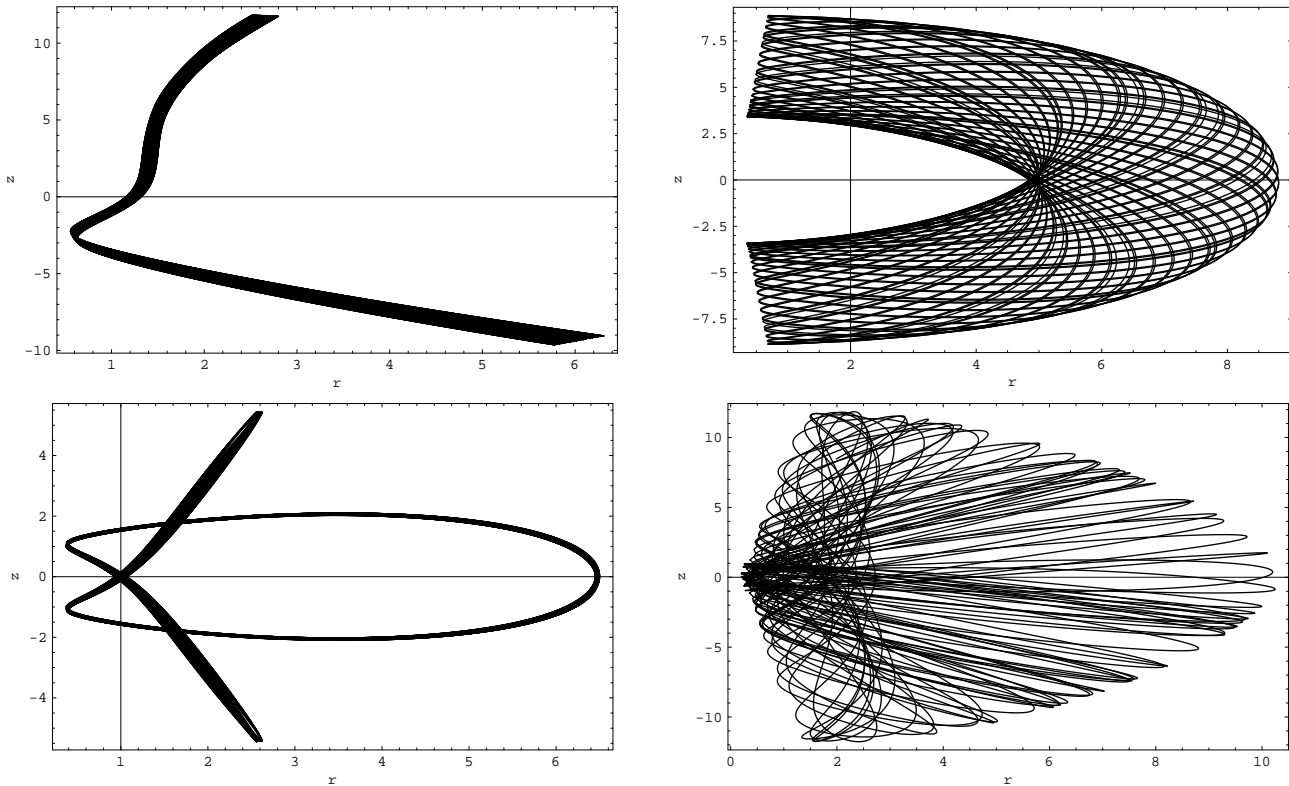


Fig. 9 (a-d): Orbits when the system has a prolate halo. (a, upper left): an orbit when $\beta = 0.2$ and $c_h = 8.5$. The initial conditions are: $r_0 = 1.3, z_0 = 0, p_{r0} = 6$. (b, upper right): a regular orbit when $\beta = 0.3$ and $c_h = 8.5$. The initial conditions are: $r_0 = 5, z_0 = 0, p_{r0} = 0$. (c, lower left): a quasi periodic orbit is shown. Here $\beta = 0.6$ and $c_h = 16$. The initial conditions are: $r_0 = 6.5, z_0 = 0, p_{r0} = 0$. (d, lower right): a chaotic orbit when $\beta = 0.2$ and $c_h = 8.5$. The initial conditions are: $r_0 = 2, z_0 = 0, p_{r0} = 0$. The values of all the other parameters are given in text.

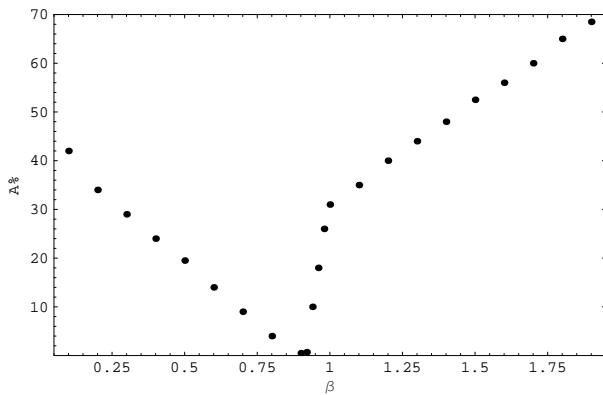


Fig. 11 A plot of the percentage of the area $A\%$ in the phase plane covered by chaotic orbits vs. β . The value of c_h is 8.5, while the values of all the other parameters are: $v_0 = 20, \alpha = 3, b = 6, h = 0.2, M_d = 5000, M_n = 400, c_n = 0.25$ and $L_z = 10$.

ure. In the first part, where $0.1 \leq \beta \leq 0.9A\%$ decreases, in the second part where $0.9 < \beta < 1.0A\%$ increases very rapidly, while in the third part where $1 < \beta < 2A\%$ also increases. An explanation for this behavior of the system will be given in the next section.

Before closing this section, we would like to present a relationship connecting the critical value of the angular momentum L_{zc} (that is the maximum value of the angular momentum, for which, stars moving near the galactic plane are scattered to the halo displaying chaotic motion, for a given value of β) and the flattening parameter β , when all the other parameters are kept constant. The results, which were found numerically, are given in Fig. 12. The value of energy is $E = 600$, while the values of all the other parameters are: $v_0 = 20, \alpha = 3, \beta = 6, h = 0.2, M_d = 5000, M_n = 400, c_n = 0.25$ and $c_h = 8.5$. We see that the relationship between β and L_{zc} is linear. Orbits starting in the upper part of the (β, L_{zc}) plane are regular, while orbits starting in the lower part of this plane including the line are chaotic. An explanation of this behavior will be given in the next section.

4 Some semi-theoretical arguments

In this section we shall present some theoretical arguments together with elementary numerical calculations in order to explain the numerically found relationships given in Figs. 11 and Fig.12. The contribution of the halo component to the chaotic regions observed in the (r, p_r) phase plane of

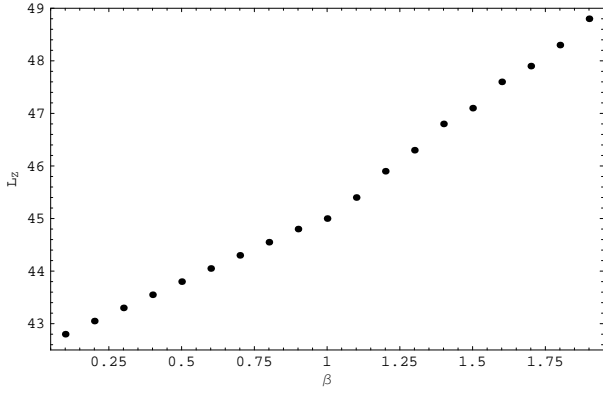


Fig. 12 A plot of the L_{zc} vs. β when $c_h = 8.5$. The value of c_h is 8.5, while the values of all the other parameters are: $v_0 = 20$, $\alpha = 3$, $b = 6$, $h = 0.2$, $M_d = 5000$, $M_n = 400$ and $c_n = 0.25$.

the system comes from two parts. The first part is the F_{zh} force, which is the vertical force of the halo and the second part comes from the asymmetry of the dark halo component. The F_{zh} force is

$$F_{zh} = \frac{-\beta v_0^2 z}{r^2 + \beta z^2 + c_h^2}, \quad (8)$$

while the asymmetry of the dark halo component can be expressed using the ellipticity (see Binney & Tremaine 2008). The ellipticity of the halo is defined as

$$\epsilon = 1 - \frac{b}{a}, \quad (9)$$

where a and b are the major and the minor axis of the biaxial halo respectively. For the prolate halo we find $\epsilon = 1 - \sqrt{\beta}$, while for the oblate halo $\epsilon = 1 - \sqrt{1/\beta}$. Figure 13 shows a plot of the $|F_{zh}|$ vs. β . As the scattering occurs near the nucleus it must be $r < 1$ and $z < 1$. The particular values of r and z are irrelevant. Here we choose $r = r_0 = 0.2$ and $z = z_0 = 0.1$. We see that $|F_{zh}|$ increases linearly with β . In the same figure a plot of ϵ vs. β is given. The value of v_0 is 20, while $c_h = 8.5$. We observe that when $0.1 \leq \beta \leq 0.9$ we have an exponential decrease of ϵ , while at the same time we have a linear increase of the $|F_{zh}|$. The result of these two contrary actions is the observed linear decrease of chaos shown in Fig. 11. When $0.9 < \beta < 1.0$ the decrease of the ellipticity can be considered linear. But at the same time, we have a considerable linear increase of the $|F_{zh}|$, which has obtained larger values. The outcome is a rapid increase of the chaotic region. When $1 < \beta < 2$, ϵ increases slowly, while the dominant role is played by the $|F_{zh}|$. As a consequence we see that the chaotic region increase to high values up to about $A\% = 70$, when β reaches 2.

The exponential decrease of the percentage of the area $A\%$ covered by chaotic orbits in the phase plane can be easily explained by plotting the $|F_{zh}|$ force, given by Eq.(8) vs. c_h , while keeping all the other parameters fixed. The results are shown in Fig. 14, where we have taken $v_0 = 20$, $\beta =$

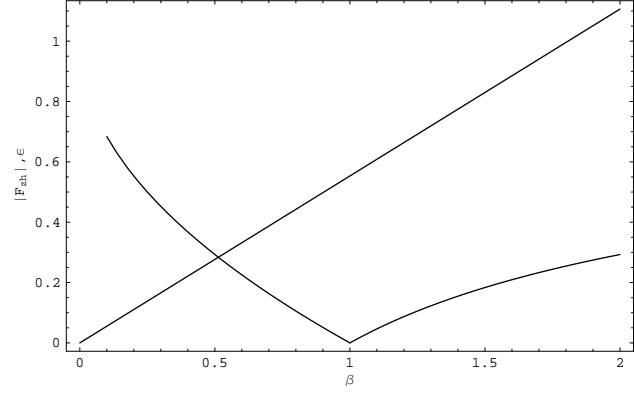


Fig. 13 A plot of $|F_{zh}|$ and ϵ vs. β . The values of all the other parameters are given in the text.

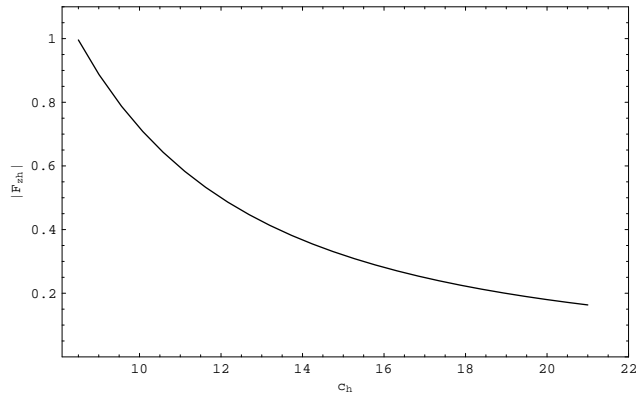


Fig. 14 A plot of $|F_{zh}|$ vs. c_h . The values of all the other parameters are given in the text.

1.8, $r = r_0 = 0.2$ and $z = z_0 = 0.1$. We see that F_{zh} decreases exponentially as c_h increases.

In order to explain the results shown in Fig. 12 we use an analysis similar to that used in Caranicolas & Innanen (1991). When the star approaches the dense nucleus its momentum in the z direction changes according to the equation

$$m\Delta v_z = \langle F_{zt} \rangle \Delta t, \quad (10)$$

where m is the mass of the star, Δt is the duration of the encounter and $\langle F_{zt} \rangle$ is the total average F_z force. It was observed that the stars deflection into higher z proceeds in each case cumulatively, a little more with each successive pass by the nucleus and not with a single “tragic” encounter. It is assumed, that the star is scattered off the galactic plane after $n > 1$ encounters when the total change in the momentum in the z direction is of order of the tangential velocity $v_\phi = L_{zc}/r$. Thus, we have

$$m \sum_{i=0}^n \Delta v_{iz} \approx \langle F_{zt} \rangle \sum_{i=0}^n \Delta t_i. \quad (11)$$

If we set $m = 1$, $\sum_{i=0}^n \Delta v_{iz} = L_{zc}/r$, $\sum_{i=0}^n \Delta t_i = T_c$ and

$$F_{zt} \approx k_1 + \frac{\beta v_0^2 |z|}{r^2 + \beta z^2 + c_h^2}, \quad (12)$$

where k_1 stands for the constant at a given point and for fixed values of the involved parameters and the vertical force coming from the nucleus and the disk components, in Eq. (11) we find

$$\frac{L_{zc}}{r} \approx k_1 + \frac{\beta v_0^2 |z| T_c}{r^2 + \beta z^2 + c_h^2}. \quad (13)$$

The star must go close to the nucleus in order to be scattered. In this case we may set $r = r_0 = |z| = c < 1$ in (13) and obtain

$$L_{zc} \approx k + \lambda \beta, \quad (14)$$

where k and λ are constants. Relation (14) explains the numerically found relationship between β and L_{zc} . The different slope in Fig. 12 for the prolate and the oblate halo can be explained because the values of c and T_c are slightly different for the two types of the dark halo component.

5 Discussion

In this article, we have tried to study the regular or chaotic character of motion in an active galaxy model with a biaxial dark halo component. It is well known from our previous work in disk galaxies with dense nuclei (see Caranicas & Innanen 1991; Caranicas & Papadopoulos 2003) that low angular momentum stars moving near the nucleus are scattered off the galactic plane displaying chaotic motion. Furthermore, this procedure is one of the main mechanism that produces chaos in galaxies (see Grosbøl 2002).

On the other hand, earlier work (Caranicas 1997; Papadopoulos & Caranicas 2006) indicates that the role of a spherically symmetric dark halo in galaxies with dense massive nuclei is to reduce the extent of the chaotic regions. It was this motive that drive us to consider a model of an active galaxy with a biaxial halo and study the dynamical effects of the additional component in the behavior of the orbits. In order to keep things simple, we have kept all the parameters of the model constant and studied the behavior of orbits varying only two basic parameters, that is the flattening parameter β and the scale length c_h of the halo. In some cases we had to find the critical value of the angular momentum in order to connect it with the flattening parameter β .

It was found that when a biaxial halo component is present there is a linear relationship between $A\%$ and the flattening parameter β . On the contrary, the relation between $A\%$ and c_h is not linear but exponential. In both cases the numerically found results were explained using some semi-theoretical arguments. In the same sense we have explained the numerically obtained relationship between L_{zc} and β .

Computation of the L.C.E shows that the degree of chaos is similar to that found for 3D time-dependent axially symmetric galactic potentials (see Caranicas & Papadopoulos 2003), where the L.C.E was about 0.5, while in 2D non axially symmetric potentials (Papadopoulos & Caranicas 2006) the L.C.E was found larger, about 1.

The main conclusion of this research is that the presence of a flattened dark halo component in an active disk galaxy has as a result to increase the extent of the chaotic regions observed in the (r, p_r) phase plane. This result is different from the results obtained in earlier papers, where the presence of the spherical halo had as a result the decrease of the chaotic region. It is in our plans, to study the behavior of orbits in active galaxy models, when a triaxial dark halo component will be present, in the near future.

Acknowledgements: The authors would like to thank the referee A. Elipe for his useful suggestions and comments.

References

- Allgood, B., Flores, R.A., et al.: 2006, MNRAS 367, 1781
 Binney, J. & Tremaine, Sc.: 2008, *Galactic Dynamics*, Princeton Series in Astrophysics, 2nd edition
 Capuzzo-Dolcetta, R., Leccese, L., et al.: 2007 ApJ 666, 165
 Caranicas, N.D.: 1997, Ap&SS 246, 15
 Caranicas, N.D., Innanen, K.A.: 1991, AJ 102, 1343
 Caranicas, N.D., Papadopoulos, N.J.: 2003, A&A 399, 957
 Cooray, A.R.: 2000, MNRAS 313, 783
 Cote, S., Wyse, R.F., et al.: 2005, ApJ 618, 178
 Dinshaw, N., Foltz, C.B., et al.: 1998, ApJ 494, 567
 Evans, N.W., An, J., et al.: 2009, ApJ 695, 1446
 Grosbøl, P.: 2002, Space Sci. Rev. 102, 73
 Jing, Y.P., Suto, Y.: 2002, ApJ 574, 538
 Kasun, S.F., Evrard, A.E.: 2005, ApJ 629, 781
 Kunihito, I., Takahiro, T., et al.: 2000, ApJ 528, 51
 Lichtenberg, A.J., Lieberman, M.A.: 1992, *Regular and Chaotic Dynamics*, Springer, 2nd edition
 McLin, K., Stocke, J.T., et al.: 2002, ApJ 574, L115
 Merritt, D., Fridman, T.: 1996, ApJ 460, 136
 Meurer, G.R., Carigan, C., et al.: 1996, AJ 11, 1551
 Olling, R.P., Merrifield, M.R.: 2000, MNRAS 311, 361
 Oppenheimer, N.C., Hambly, A.P. et al.: 2001, Sci 292, 698
 Papadopoulos, N.J., Caranicas, N.D.: 2006, New A 12, 11
 Penton, S.V., Stocke, J.T., Shull, J.M.: 2002, ApJ 565, 720
 Shull, J.M., Penton, S.V., et al.: 1998, AJ 116, 2094
 Steidel, C.C., Kollmeier, J.A., et al.: 2002, ApJ 570, 526
 Wang, H., Mo, H.J., et al.: 2009, MNRAS 394, 398
 Wechsler, R.H., Bullock, J., et al.: 2002, ApJ 568, 52